The Meteoritical Society

Meteoritics & Planetary Science 56, Nr 11, 2002–2016 (2021)
doi: 10.1111/maps.13760

Light noble gas records and cosmic ray exposure histories of recent ordinary chondrite falls

Thomas SMITH[1]*, Huaiyu HE[1,2,3]*, Shijie LI[4], P. M. RANJITH[1], Fei SU[1,2], Jérôme GATTACCECA[5], Régis BRAUCHER[5], and ASTER-Team[5,†]

[1]State Key Laboratory of Lithospheric Evolution, Institute of Geology and Geophysics, Chinese Academy of Sciences, Beijing 100029, China
[2]Institutions of Earth Science, Chinese Academy of Sciences, Beijing 100029, China
[3]College of Earth and Planetary Sciences, University of Chinese Academy of Sciences, Beijing 100049, China
[4]Center for Lunar and Planetary Sciences, Institute of Geochemistry, Chinese Academy of Sciences, Guiyang 550081, China
[5]Centre Européen de Recherche et d'Enseignement de Géosciences de l'Environnement (CEREGE), CNRS, Aix-Marseille University, IRD, INRAE, Aix-en-Provence, France
*Corresponding authors. E-mail: thomas.smith@mail.iggcas.ac.cn; huaiyuhe@mail.iggcas.ac.cn

(Received 11 November 2020; revision accepted 30 September 2021)

Abstract–We measured noble gas concentrations and isotopic ratios (He, Ne, and Ar isotopes) in six recent ordinary chondrite falls: Mangui (L6), Viñales (L6), Ozerki (L6), Tamdakht (H5), Kheneg Ljouâd (LL5/6), and Katol (L6). Among them, the three L6 chondrites Mangui, Viñales, and Ozerki fell in only a few months' interval; their apparent similar petrographic and mineralogic characteristics might indicate source crater pairing. To test this hypothesis, we have investigated those meteorites for their cosmic ray exposure (CRE) histories, using the cosmogenic noble gases ^{3}He, ^{21}Ne, and ^{38}Ar. We systematically (re)calculated the CRE ages as well as the gas retention ages of these meteorites. The CRE age of the Mangui is, based on noble gases, <1 Ma, which is unusually short for an L chondrite. Indeed, the range of exposure ages for L chondrites is generally distributed between ~1 and ~60 Ma, with major peaks occurring around ~5, ~30, and ~40 Ma. In addition, the cosmogenic $^{3}He_{cos}$ data of two Mangui duplicates are consistent with a remarkably high loss of helium by diffusion due to heating by solar radiation. Such a short parent body-Earth transfer time (<1 Ma) can be explained by a delivery from an Earth-crossing object. Regarding the other L6 chondrites, Viñales has a nominal CRE age of ~9.4 Ma, whereas the Ozerki meteorite has a nominal CRE age of ~1.2 Ma, which is consistent with Korochantseva et al. (2019). Based on their CRE ages as well as on their gas retention ages, it appears that none of these three recent L6 chondrite falls are source crater paired, and therefore, all three originate from different meteoroids. The nominal exposure ages of Tamdakht, Kheneg Ljouâd, and Katol are ~3.2, ~11, and ~30 Ma, respectively, and are consistent with identified age peaks on the exposure age histogram of H, LL, and L chondrites, respectively. The nominal CRE age of Tamdakht is consistent with previous observations for H chondrites and implies that they are dominated by small impact events occurring in several parent bodies.

INTRODUCTION

Cosmogenic noble gases (i.e., He, Ne, Ar, Kr, and Xe) and radionuclides (i.e., ^{10}Be, ^{26}Al, ^{36}Cl, ^{41}Ca, among others) in meteorites are formed by the interaction of highly energetic galactic particles (galactic cosmic rays, hereafter labeled GCRs) and meteoroids in space or at the surface of airless planetary bodies. The isotopic abundance of cosmogenic radionuclides in meteorites is controlled by (1) their chemistry, that is, the abundance of the relevant target elements; (2) their

[†]Georges Aumaître, Didier L. Bourlès, and Karim Keddadouche are part of the ASTER-Team.

depth within their parent body (shielding depth); and (3) the time they have been irradiated in space after breakup from their parent body, that is, their cosmic ray exposure (CRE) age. With a comprehensive data set of cosmogenic nuclides in a meteorite sample, it is possible to have access to the full irradiation history (CRE age and terrestrial age) as well as the preatmospheric size and the shielding depth of the meteorite. Whereas CRE ages of meteorites can provide insights about the constancy of GCRs (e.g., Lavielle et al., 1999; Moniot et al., 1983; Shaviv, 2002, 2003; Smith et al., 2019; Vogt et al., 1993; Wieler et al., 2013), their calculation has implications on major questions regarding the delivery mechanisms of meteorites to the Earth, for example, the investigation of the collisional processes on the parent bodies which have created the known meteorites of each types (e.g., Herzog, 2007; Herzog & Caffee, 2014). CRE age histograms for all meteorite groups, based on a (more or less extensive) set of CRE ages, lead to the determination of the age distribution patterns and identify major impact events in the parent bodies responsible for the supply of meteorites to the Earth. However, statistics are rather significant for some groups of meteorites, for example, L chondrites or some of the H chondrites, leading to the identification of major disruption events in their respective parent bodies; other groups with rarer meteorites have been less extensively studied, for example, the LL chondrites for which data are less comprehensive (Herzog, 2007; Herzog & Caffee, 2014).

Although the terrestrial ages of most of the meteorite finds are orders of magnitude smaller than their exposure ages (e.g., Jull, 2001), CRE ages of meteorite falls have the advantage of directly representing the ejection time from the parent body. A relatively large number of chondrite falls have been observed in 2018 and 2019. Among them, we obtained samples of three meteorites: Mangui from China, Ozerki from Russia, and Viñales from Cuba. The Mangui meteorite (L6) fell in the Yunnan Province, China, at 9:43 P.M. on June 1, 2018 (Ji et al., 2018). Based on recent calculations, the meteorite entered Earth's atmosphere with an angle of 55.3 ± 2.5°, from southeast to northwest, resulting in a strewn field of ~12 km long (Li et al., 2020). To date, more than 1000 individuals or fragments have been identified, with masses ranging from 0.04 g to ~1280 g, the total mass being ~50 kg. The Ozerki meteorite (L6) fell in Russia, near the city of Lipetsk, on June 21, 2018, that is, 20 days after the Mangui fall. Based on models, the total number of specimens is estimated to be ~100, for a total mass of >10 kg (Korochantseva et al., 2019). The first studies conducted on Ozerki indicate the absence of heavy particle tracks in olivine grains, which has been interpreted as an indication of a low CRE age (Efimov et al., 2019). Finally, the Viñales meteorite (L6) fell in Cuba on February 1, 2019. In the following days, hundreds of individual specimens were collected by locals. Here, we study the CRE history of two individual samples of Mangui, Ozerki, and Viñales by measuring cosmogenic noble gas isotopes produced in space by GCRs. Based on the similar petrographic types between these different observed falls and on their similar shock characteristics, it is possible that these three meteorites might have been ejected from the same crater on the L-chondrite parent body. In addition to these three fresh-fallen L6 chondrites, we investigated the exposure history of the Katol (L6) chondrite: on May 22, 2012, around 2:10 P.M. local time, a large meteor shower occurred over the town of Katol located in the Nagpur District of Maharashtra, India. Based on the description in the Meteoritical Bulletin Database, the largest recovered mass is ~1 kg, for a total recovered mass being >13 kg. Katol, classified as an L6 chondrite, has an apparent shock stage of S5, but the silicates indicate a rather lower shock stage of S2 (Ruzicka et al., 2015).

Among the 67 records of LL5/6 meteorites, Kheneg Ljouâd represents the only witnessed fall. The distribution of the exposure ages of LL chondrites is as follows: CRE ages range from 0.5 to 80 Ma, with an apparent peak around ~15 Ma (Herzog, 2007; Herzog & Caffee, 2014). It is still not clear whether the different types of LL chondrites contribute to different peaks in the CRE age histogram. Therefore, we investigated the exposure history of the fresh-fallen LL5/6 Kheneg Ljouâd meteorite to evaluate if its CRE age fits into the existing established exposure histograms. On July 12, 2017, Kheneg Ljouâd fell; around 11 P.M. Moroccan time (GMT+1), a bright fireball was widely seen throughout southern Morocco, travelling from the NE to the SW, with the termination of the fireball southwest of Tata. The largest complete piece was about 850 g, for a total known recovered mass of ~10 kg. The observation of a few small melt pockets is consistent with shock stage S3.

The fall of Tamdakht (H5), one of the 183 H5 falls, was witnessed on December 20, 2008, from a number of different locations in Morocco (Agadir, Marrakesh, Ouarzazate). Several impacts were detected: the largest, located near Oued Aachir (1.10 m diameter and 70 cm depth), with a recovered single mass of >30 kg and many small fragments, and a second (~20 cm diameter and 10 cm depth) located 2 km W from the first one; the main mass from the second impact was probably about 500 g. Nine new impact coordinates were reported, forming a strewn field of ~25 km long and ~2 km wide. Based on the description in the Meteoritical Bulletin Database, the total known weight is estimated to be around 100 kg.

Table 1. Description of the meteorites studied in this work: meteorite group, petrologic type, date of fall, total known weight, shock stage, and mineralogy.

Meteorite name	Classification	Date of fall	Total known weight (kg)	Shock stage	Fa (mol%)	Fs (mol%)
Mangui	L6	June 1, 2018	50	S4–S5	24.7 ± 0.2	21.0 ± 0.2
Ozerki	L6	June 21, 2018	6.5, >10	S4–S5	25.6 ± 0.3	21.4 ± 0.2
Viñales	L6	February 1, 2019	50	S3	24.7 ± 0.3	21.0 ± 0.4
Katol	L6	May 22, 2012	>13	S2–S5	24.9 ± 0.4	21.9 ± 0.5
Kheneg Ljouâd	LL5/6	July 12, 2017	10	S3	31.0 ± 0.2	25.0 ± 0.4
Tamdakht	H5	December 20, 2008	100	S3	18.0 ± 0.5	16

Fa = fayalite; Fs = ferrosilite.

We report in this paper the CRE history of these recent chondrite falls, with a systematic calculation of their CRE ages, and U-Th-He and K-Ar gas retention ages. This set of data will help to better constrain their delivery mechanisms to Earth from the asteroid belt and highlight links with the major breakup events of the ordinary chondrite parent body(-ies).

SAMPLES AND THEIR PETROGRAPHY AND MINERALOGY

The description of the meteorites studied in this work, including their petrologic type, the date of fall, the total known weight, their shock stage, and their fayalite and ferrosilite contents are summarized in Table 1. We here briefly summarize it.

Mangui (L6)

The detailed petrography and mineralogy of Mangui are reported in Ji et al. (2018) and Li et al. (2020). Mangui has been classified as an L6 ordinary chondrite, with a shock stage S4–S5, with rare chondrules (Ji et al., 2018; Li et al., 2020). In addition, some high-pressure minerals were also observed in some of the polished sections of the Mangui meteorite.

Viñales (L6)

The petrography of Viñales was given in Gattacceca et al. (2020b). Distinguishable chondrules were observed in the polished thin section of Viñales. In addition, various shock-related characteristics such as shock veins, well-developed fractures, and small blebs of Fe-Ni and troilite mixture have been observed in Viñales. The shock stage is S3–S4 (Yin & Dai, 2021).

Katol (L6)

The basic information of the meteorite Katol is reported in Ruzicka et al. (2015). Shock-induced features such as planar fractures, planar deformation features in olivine, and mineral transformations, such as plagioclase–maskelynite and olivine–wadsleyite/ringwoodite, have been documented in a study on the possible origin of troilite metal nodules in the Katol meteorite (Ray et al., 2017).

Ozerki (L6)

The detailed petrography and geochemistry information of Ozerki is reported in Gattacceca et al. (2020a). Ozerki is an L6 ordinary chondrite, with rare relic chondrules, with a shock stage of S4–S5.

Tamdakht (H5)

The Tamdakht meteorite is described in Weisberg et al. (2009). The stone contains abundant chondrules, but the outlines of the chondrules are not clear.

Kheneg Ljouâd (LL5/6)

A preliminary study of LL5/6 ordinary chondrite Kheneg Ljouâd was reported by Aoudjehane Chennaoui and Garvie (2018). A few shock melt pockets indicate Kheneg Ljouâd suffered a shock degree of S3.

EXPERIMENTAL PROCEDURES

Noble Gases

Two duplicates of Mangui, Ozerki, and Viñales have been analyzed for light noble gas (He, Ne, and Ar) concentrations and isotopic ratios. In addition, three aliquots of the meteorite Katol have been measured. We hereafter call these series of aliquots "Mangui-1" and "Mangui-2"; "Ozerki-1" and "Ozerki-2"; "Viñales-1" and "Viñales-2"; and "Katol-1," "Katol-2," and "Katol-3." Note that all of those aliquots are extracted from the same fragment of the respective meteorite.

The samples have been measured for light noble gas isotopes in the noble gas laboratory at the Institute of Geology and Geophysics, Chinese Academy of Sciences (IGGCAS), Beijing, China. The

noble gas concentrations and isotopic ratios (^{3,4}He, ^{20,21,22}Ne, and ^{36,38,40}Ar) have been measured using a multi-collector noble gas mass spectrometer Noblesse© from Nu Instruments. The analytical procedures follow the same procedures as described previously in Ranjith et al. (2017). Briefly, bulk samples with masses ranging from ~4 to ~8 mg were first cleaned with ethanol in an ultrasonic bath, dried, weighed, and then loaded into the laser sample chamber of the noble gas extraction and purification line. Samples with small masses are more suitable for laser heating extraction than samples with larger masses (~20–100 mg), usually preferred for RF furnace heating extraction. The whole system was baked and evacuated for ~3 days at ~120 °C in order to remove adsorbed atmospheric gases.

Before sample measurements, calibrations were performed using standard gases, which, except for He, are of atmospheric composition. The He standard is the "He Standard of Japan" (HESJ) with a well-calibrated ^{3}He/^{4}He ratio of 20.6 ± 0.1 Ra (Matsuda et al., 2002), where Ra stands for the ^{3}He/^{4}He ratio of air (i.e., Ra = 1.4×10^{-6}). Sensitivities and instrumental mass discriminations have been calculated based on the air measurements carried out at the time when the samples were analyzed.

Blanks have been frequently measured using the exact same extraction procedure as for the samples (see details below). Typically, they contribute to <1% for He, <2% for Ne, and <5% for Ar isotopes.

Noble gases have been extracted by heating the sample chips in either a single extraction step or a stepwise heating, using a CO_2 laser (1.064 μm wavelength, default setting with a 2–3 mm diameter beam size) for ~30 min. The released gases were first cleaned from all reactive gases that would compromise the measurements, such as CO_2, H_2O, or hydrocarbons, using a series of getters, operating at room temperature and 200 °C (Ranjith et al., 2017). The He-Ne fraction was separated from the Ar fraction using an activated charcoal trap held at LN_2 temperature for 20 min. Subsequently, the Ne fraction was separated from the remaining He using a cryogenic cold trap held at 35 K for 10 min. A fraction of the He gas was then introduced into the mass spectrometer. The Ne fraction was released at 80 K for 30 min and the total gas fraction was then introduced into the mass spectrometer; remaining background gases, especially $^{40}Ar^{++}$ and $^{44}CO_2^{++}$ interfering at m/e = 20 and m/e = 22, respectively, which would compromise the Ne measurements, are further reduced using a charcoal trap held at LN_2 temperature during the measurement. Finally, Ar was released at ~150 °C for 20 min, and a known fraction of the gas was measured. After the first measurement, second extractions at a slightly higher laser power were systematically performed in order to ensure that samples were completely degassed. The second extractions contribute generally for ~1% for He, ~10% for Ne, and ~5–7% for Ar. Second extraction contributions were added to the total amount of He, Ne, and Ar; the total amount of extracted gases was subsequently corrected for blank.

Major and Minor Elements

The major and trace element analyses of Mangui, Viñales, and Ozerki were performed at Guizhou Tongwei Analytical Technology Co., Ltd. Trace elements were measured using a Thermo Scientific XSeries 2 inductively coupled plasma mass spectrometer (ICP-MS) equipped with a Cetac ASX-510 Auto Sampler. Powders of aliquots of 50–100 mg each were dissolved in a Teflon bomb with double-distilled concentrated HNO_3-HF (1:4) mixture. Samples have been dissolved in an oven at 185 °C for 3 days. The solutions were then evaporated to dryness in order to remove HF. The sample residues were re-dissolved with double-distilled concentrated (45%) HNO_3 and dried again. Then, the samples were dissolved in a 3 mL 2N HNO_3 solution. Finally, the solution was diluted to 4000 times with 2% HNO_3 along with the addition of internal carrier solutions of 10 ppb of ^{61}Ni, 6 ppb of Rh, as well as In and Re. The United States Geological Survey standard W-2a has been used as reference material and cross-calibrated with other reference materials such as BIR-1 and BHVO-2. Instrument drift mass bias was corrected with internal spikes. The ICP-MS procedure for trace element analysis follows the protocol of Eggins et al. (1997) with some modifications as described in Kamber et al. (2003) and Li et al. (2005).

RESULTS

The measured isotopic noble gas concentrations of the six ordinary chondrites corrected for blank (by removing the amounts of each isotope measured in blanks), for interference from H_2O^+, $^{40}Ar^{++}$, and CO_2^{++} on Ne isotopes, and for instrumental mass discrimination are presented in Table 2.

Helium

Concentrations

It is assumed that all measured ^{3}He is cosmogenic, based on the measured ^{4}He concentration and cosmogenic Ne composition (e.g., Alexeev, 1998). The cosmogenic $^3He_{cos}$ concentrations in all duplicates are in good agreement with each other. Within their respective uncertainties (2σ), all duplicates of each sample show reproducible concentrations. The measured concentration,

Table 2. Analyzed mass of the studied samples and their He, Ne, and Ar concentrations and isotopic ratios.

Samples	Mass (mg)	^{3}He (10^{-8} cm^3 STP g^{-1})	$^{3}He/^{4}He$	^{20}Ne (10^{-8} cm^3 STP g^{-1})	$^{20}Ne/^{22}Ne$	$^{21}Ne/^{22}Ne$	^{38}Ar ($10^{-8}cm^3$ STP g^{-1})	$^{36}Ar/^{38}Ar$	$^{40}Ar/^{36}Ar$
Mangui-1	6.62	0.271 ± 0.014	0.054 ± 0.001	0.491 ± 0.025	1.367 ± 0.005	0.883 ± 0.003	0.093 ± 0.005	3.012 ± 0.008	155 ± 2
Mangui-2	7.36	0.233 ± 0.012	0.096 ± 0.002	0.416 ± 0.021	1.528 ± 0.006	0.858 ± 0.004	0.062 ± 0.003	3.135 ± 0.012	197 ± 3
Ozerki-1	6.31	2.324 ± 0.116	0.0038 ± 0.0006	0.551 ± 0.028	0.961 ± 0.002	0.927 ± 0.003	0.158 ± 0.008	2.038 ± 0.030	19,148 ± 277
Ozerki-2	4.86	2.134 ± 0.107	0.0022 ± 0.0006	0.594 ± 0.030	1.149 ± 0.004	0.911 ± 0.003	0.146 ± 0.007	3.944 ± 0.057	11,286 ± 164
Viñales-1	5.57	17.03 ± 0.85	0.061 ± 0.001	3.385 ± 0.169	0.862 ± 0.002	0.933 ± 0.002	0.534 ± 0.027	1.868 ± 0.027	222 ± 4
Viñales-2	5.47	17.01 ± 0.85	0.068 ± 0.002	3.541 ± 0.177	0.864 ± 0.002	0.930 ± 0.002	0.505 ± 0.025	1.190 ± 0.017	516 ± 10
Tamdakht	3.86	4.982 ± 0.249	0.0033 ± 0.0002	1.017 ± 0.116	0.927 ± 0.002	0.868 ± 0.001	0.218 ± 0.011	3.102 ± 0.049	7689 ± 111
Kheneg Ljouâd	7.45	17.71 ± 0.89	0.011 ± 0.001	3.656 ± 0.183	0.850 ± 0.002	0.888 ± 0.002	0.541 ± 0.027	1.315 ± 0.019	10,454 ± 151
Katol-1	6.30	43.06 ± 2.15	0.056 ± 0.001	10.38 ± 0.52	0.828 ± 0.017	0.939 ± 0.019	0.597 ± 0.030	1.914 ± 0.038	6753 ± 135
Katol-2	4.91	45.49 ± 2.27	0.106 ± 0.002	11.34 ± 0.57	0.827 ± 0.017	0.930 ± 0.019	0.737 ± 0.037	0.832 ± 0.017	9639 ± 193
Katol-3	4.98	43.80 ± 2.19	0.090 ± 0.002	10.39 ± 0.52	0.828 ± 0.017	0.929 ± 0.019	0.843 ± 0.042	1.475 ± 0.030	3149 ± 63

Data are corrected for blanks, instrumental mass discrimination, and interferences. Since noble gas mass spectrometers are optimized for isotope ratio measurements, the uncertainties caused by the extrapolation are very often much smaller for isotope ratios than for individual isotopes.

$^4He_{meas,}$ is assumed as the sum of the radiogenic and cosmogenic (hereafter labeled with the index "cos") contributions such as:

$$^4He_{meas} = {}^4He_{rad} + (^4He/^3He)_{cos} \times {}^3He_{cos},$$

where $^4He_{rad}$ stands for the radiogenic ^4He produced in situ from the radioactive decay of U, Th, and Sm, and $(^4He/^3He)_{cos}$ is the cosmogenic He isotopic ratio. This ratio ranges from ~5.1 to 6.7 (Alexeev, 1998), and in agreement with modeled $(^4He/^3He)_{cos}$ ratios in H chondrites (with preatmospheric radii between 10 and 120 cm), with an average modeled $(^4He/^3He)_{cos}$ of 5.6 ± 0.5 (Leya & Masarik, 2009).

Isotopic Ratios

After blank corrections, the two Mangui duplicates have $^3He/^4He$ ratios of 5.54×10^{-2} and 9.63×10^{-2}; assuming no or only little variation in the chemical composition of the two duplicates, this variation can be explained by greater He diffusive losses in "Mangui-1." For Ozerki, the two measured duplicates have $^3He/^4He$ ratios of 2.17×10^{-3} and 3.83×10^{-3}. As for Viñales, the two samples have reproducible $^3He/^4He$ ratios of 6.13×10^{-2} and 6.81×10^{-2}. The $^3He/^4He$ ratios in the three Katol aliquots range from 5.60×10^{-2} to 1.06×10^{-1}. These ratios are all lower than the expected purely cosmogenic $^3He/^4He$ ratios, which are, on average, varying between 0.149 and 0.196 (Alexeev, 1998). Such differences could be explained by diffusion losses of He (see the Discussion section) and by evoking the presence of radiogenic $^4He_{rad}$.

Neon

Concentrations

The measured neon concentrations and isotopic ratios are given in Table 2. The concentrations have been corrected for fractionation and interferences, but we did not correct the data for any blank (which is of atmospheric composition) since we will apply a two-component deconvolution for later corrections (see the Discussion section). For all studied duplicates, the measured $^{20}Ne_m$ concentrations are, in general, consistent with each other, before any component corrections. Each duplicate of Ozerki, Viñales, and Katol gives consistent concentrations within their respective uncertainties. However, the two Mangui duplicates show some variations of ~20% on average.

Isotopic Ratios

The measured $^{20}Ne/^{22}Ne$ ratios in the samples vary between ~0.83 for Katol and 1.53 for one of the two Mangui duplicates. Although the measured $^{20}Ne/^{22}Ne$ ratios for Katol, Kheneg Ljouâd, and Viñales appear to be purely cosmogenic, the two Mangui duplicates and Ozerki-2 have $^{20}Ne/^{22}Ne$ ratios greater than 1, which is usually interpreted as addition of trapped (probably atmospheric) Ne in the samples; however, these meteorites being fresh falls, the presence of significant trapped Ne component is rather unusual. It can, however, be explained by contribution from the Ne blank in the purification line combined with low cosmogenic Ne concentrations.

Argon

The measured Ar isotopic ratios $^{40}Ar/^{36}Ar$ and $^{38}Ar/^{36}Ar$ are given in Table 2. The measured $^{36}Ar/^{38}Ar$ ratios in Mangui, Ozerki, Viñales, and Katol range from 3.01 to 3.13, 2.04 to 3.94, 1.19 to 1.87, and 0.83 to 1.91, respectively (two and three duplicates have been measured for Mangui, Ozerki, Viñales, and Katol, respectively). The two meteorites Kheneg Ljouâd and Tamdakht have $^{36}Ar/^{38}Ar$ ratios ranging from 1.32 and 3.10, respectively. These elevated ratios, compared to cosmogenic $(^{36}Ar/^{38}Ar)_{cos} = 0.63$, are consistent with variable amounts of trapped atmospheric argon in the samples. The $^{40}Ar/^{36}Ar$ ratios vary between ~155–197, ~11,300–19,150, and ~222–516 for Mangui, Ozerki, and Viñales, respectively. The high $^{40}Ar/^{36}Ar$ ratios measured in Ozerki can be explained by radiogenic production from high concentrations of K. Similar to Ozerki, the two chondrites Tamdakht and Kheneg Ljouâd have high $^{40}Ar/^{36}Ar$ ratios of ~7700 and ~10,500, respectively, associated with high $^4He/^3He$ of ~91 and ~303. The measured $^{40}Ar/^{36}Ar$ ratios in the three duplicates of Katol show more discrepancies, with variations between ~3150 and ~9600, which may indicate highly heterogeneous radiogenic ^{40}Ar.

DISCUSSION

Cosmogenic Concentrations

Neon

The measured $^{20}Ne/^{22}Ne$ ratios in our samples vary between ~0.83 for Katol and 1.53 for one of the two Mangui duplicates (Table 2; Fig. 1). The results suggest a mixture between a cosmogenic component with a $^{20}Ne/^{22}Ne$ ~0.85 and a minor contribution from a trapped component, most likely terrestrial atmosphere (with $^{20}Ne/^{22}Ne = 9.80$). No evidence of a solar component is observed. The cosmogenic Ne concentrations and isotopic ratios are reported in Table 3; here, we used a two-component deconvolution with $(^{20}Ne/^{22}Ne)_{cos} = 0.83$ (i.e., Leya et al., 2013), which corresponds to the lowest ratio measured for our samples and trapped—atmospheric—

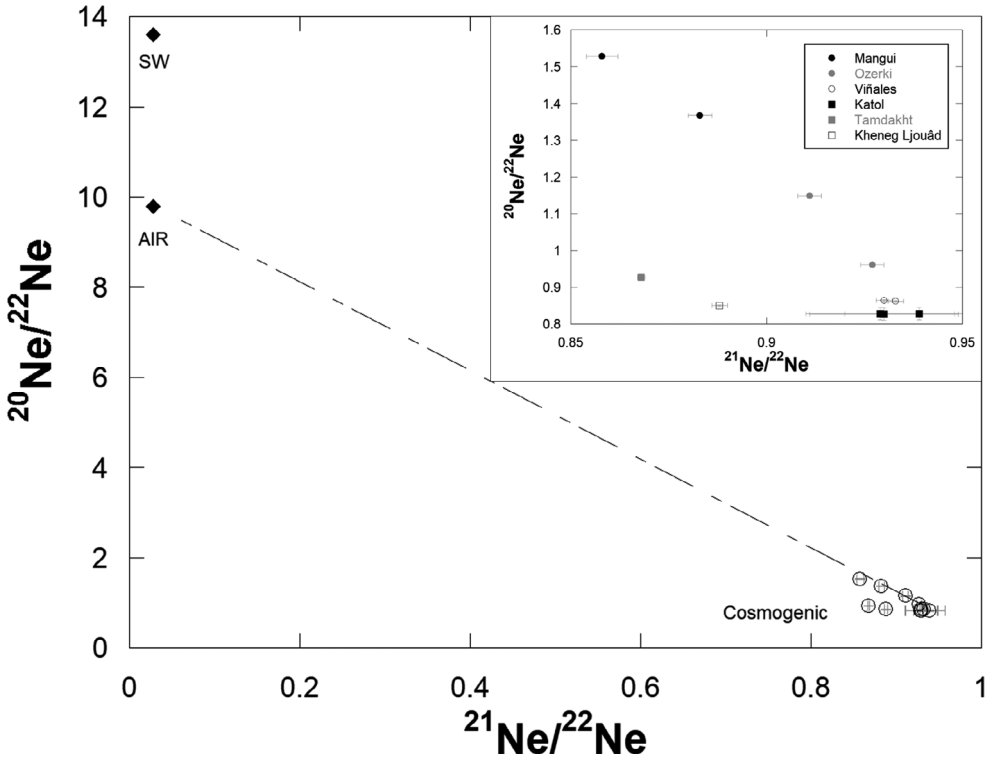

Fig. 1. Neon three-isotope plot for the measured samples. Trapped component endmembers (air and solar wind—SW) are represented by solid diamonds. Dashed line represents the mixing line between air and pure cosmogenic components for chondrites. Error bars are 2 standard deviations.

Table 3. Cosmogenic (cos) He, Ne, and Ar concentrations (in 10^{-8} cm^3 STP g^{-1}) and isotopic compositions, and radiogenic (rad) $^4He_{rad}$.

Samples	$^3He_m = {}^3He_{cos}$ (10^{-8} cm^3 STP g^{-1})	$^4He_{rad}$ (10^{-8} cm^3 STP g^{-1})	$^{21}Ne_{cos}$ (10^{-8} cm^3 STP g^{-1})	$(^{22}Ne/^{21}Ne)_{cos}$	$^{36}Ar_{cos}$ (10^{-8} cm^3 STP g^{-1})	$^{38}Ar_{cos}$ (10^{-8} cm^3 STP g^{-1})
Mangui-1	0.271 ± 0.014	3.411 ± 0.255	0.317 ± 0.022	1.087 ± 0.059	0.027 ± 0.002	0.043 ± 0.003
Mangui-2	0.233 ± 0.012	1.193 ± 0.089	0.233 ± 0.016	1.098 ± 0.059	0.015 ± 0.001	0.024 ± 0.002
Ozerki-1	2.324 ± 0.116	593 ± 44	0.532 ± 0.038	1.062 ± 0.057	0.070 ± 0.005	0.110 ± 0.008
Ozerki-2	2.134 ± 0.107	969 ± 72	0.471 ± 0.033	1.058 ± 0.057	0.027 ± 0.002	0.043 ± 0.003
Viñales-1	17.03 ± 0.85	178 ± 13	3.662 ± 0.259	1.067 ± 0.057	0.248 ± 0.018	0.393 ± 0.028
Viñales-2	17.01 ± 0.85	151 ± 11	3.809 ± 0.269	1.070 ± 0.059	0.280 ± 0.020	0.445 ± 0.031
Tamdakht	4.982 ± 0.249	1466 ± 109	0.951 ± 0.067	1.139 ± 0.061	0.065 ± 0.005	0.103 ± 0.007
Kheneg Ljouâd	17.71 ± 0.89	1504 ± 112	3.817 ± 0.270	1.123 ± 0.060	0.291 ± 0.021	0.462 ± 0.033
Katol-1	43.06 ± 2.15	768 ± 57	11.89 ± 0.84	1.065 ± 0.057	0.288 ± 0.020	0.443 ± 0.031
Katol-2	45.49 ± 2.27	428 ± 32	12.66 ± 0.90	1.075 ± 0.058	0.460 ± 0.033	0.708 ± 0.050
Katol-3	43.80 ± 2.19	487 ± 36	11.66 ± 0.82	1.077 ± 0.058	0.444 ± 0.031	0.683 ± 0.048

$(^{20}Ne/^{22}Ne)_{trap}$ = 9.80. Unlike Korochantseva et al. (2019), we did not consider a third component in Ozerki (i.e., SW) to calculate the cosmogenic Ne concentrations and isotopic ratios. All cosmogenic Ne concentrations and ratios are given in Table 3. The corrections for ^{21}Ne are, for all samples, negligible and <1%. The corrected $(^{22}Ne/^{21}Ne)_{cos}$ ratios for all samples vary between 1.058 and 1.139, which is well within the range of ratios expected for cosmogenic Ne production in chondrites (e.g., Leya et al., 2013). However, lower end values in such ratios might indicate, at first sight, a large preatmospheric size.

Helium Diffusive Losses

Helium diffusive losses by heating during the exposure of the meteorites to solar radiation while in orbits with small perihelion distances can be inferred

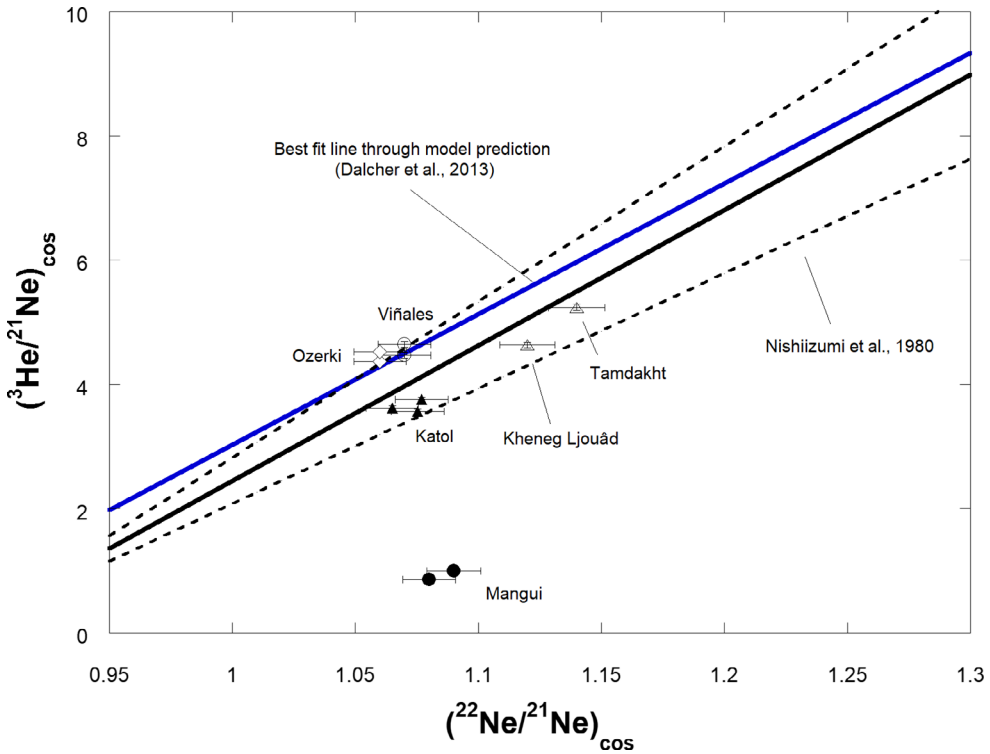

Fig. 2. Cosmogenic $^3He/^{21}Ne$ versus $^{22}Ne/^{21}Ne$ (so-called "Bern plot"). The data for the two Mangui, Viñales, Ozerki, Katol, Tamdakht, and Kheneg Ljouâd samples are reported here. The solid black line represents the empirical correlation for chondrites given by Nishiizumi et al. (1980). The black dashed lines represent the ±15% variations from the correlation. The best-fit line through model predictions from Dalcher et al. (2013) is shown in blue. (Color figure can be viewed at wileyonlinelibrary.com.)

from the so-called "Bern-plot," a plot of $^3He/^{21}Ne$ versus $^{22}Ne/^{21}Ne$ (Nishiizumi et al., 1980) (Fig. 2). To estimate such potential He losses in our samples, we plotted the data, and we used the empirical correlation line obtained with the data of 138 L and H chondrites (Nishiizumi et al., 1980), as well as the best-fit line obtained with the model of Leya and Masarik (2009) for L chondrites with radii <65 cm and assuming an atmospheric ablation loss of 85% (Bhandari et al., 1980). More details about that model can be found in Dalcher et al. (2013). In Fig. 2, both Mangui duplicates plot far below the empirical correlation line $^3He/^{21}Ne$ versus $^{22}Ne/^{21}Ne$ and the model predictions, therefore suggesting that the meteorite lost a significant amount of $^3He_{cos}$; based on that plot, we estimate that ~55–75% of the initial total He has been lost, whereas both duplicates of Ozerki and Viñales plot within the ±15% error envelope of the empirical correlation line; in addition, both Ozerki and Viñales samples plot on the best-fit line through model predictions. This suggests that both Ozerki and Viñales have only suffered little or negligible He losses. As do Ozerki and Viñales, the three duplicates of the Katol meteorite plot perfectly within the ±15% error envelope of the empirical correlation line, consistent with no or only little loss of He. Tamdakht and Kheneg Ljouâd plot both close to the correlation line of Nishiizumi et al. (1980), suggesting that no significant He losses occurred during the exposure histories of these two meteorites.

Argon

The wide range of measured $^{36}Ar/^{38}Ar$ ratios (0.83–3.94, Table 2) in all the samples measured here clearly indicates the presence of a trapped component, most likely atmospheric, in addition to the cosmogenic component. We used a classical two-component deconvolution assuming that the isotopic compositions are a mixture between cosmogenic and terrestrial air endmembers. Thus, we used the following assumptions: $(^{36}Ar/^{38}Ar)_{cos} = 0.63$ and $(^{36}Ar/^{38}Ar)_{air} = 5.32$ (Leya et al., 2013). The cosmogenic $^{36}Ar_{cos}$ and $^{38}Ar_{cos}$ concentrations are reported in Table 3. The average correction for $^{36,38}Ar$ is ~34%, with variations between ~4% (Katol) and ~70% (Ozerki).

Major and Minor Elements

The major and trace elemental compositions in the meteorites Mangui, Viñales, and Ozerki are reported in Appendix S1 in the supporting information. The element distribution, normalized to CI chondrites, is

Table 4. Cosmic ray exposure (CRE) ages for the measured chondrites.

Samples	Mass (mg)	T_3 (Ma)	T_{21} (Ma)	T_{38} (Ma)	Average (Ma)	$T_{adopted}$ (Ma)
Mangui-1	6.62	(0.17 ± 0.02)	0.78 ± 0.09	0.88 ± 0.10	0.83 ± 0.13	**0.70 ± 0.16**
Mangui-2	7.36	(0.14 ± 0.02)	0.61 ± 0.07	0.52 ± 0.06	0.57 ± 0.09	
Ozerki-1	6.31	1.42 ± 0.16	1.15 ± 0.13	1.32 ± 0.15	1.30 ± 0.29	**1.30 ± 0.29**
Ozerki-2	4.86	1.31 ± 0.15	1.00 ± 0.11	(0.55 ± 0.06)	1.16 ± 0.19	
Viñales-1	5.57	10.4 ± 1.2	8.13 ± 0.93	(4.65 ± 0.53)	9.27 ± 1.51	**9.39 ± 2.16**
Viñales-2	5.47	10.4 ± 1.2	8.59 ± 0.98	(5.34 ± 0.61)	9.50 ± 1.54	
Tamdakht	3.86	3.11 ± 0.36	3.37 ± 0.38	2.59 ± 0.44	3.02 ± 0.71	**3.02 ± 0.71**
Kheneg Ljouâd	7.45	11.0 ± 1.3	11.2 ± 1.3	10.9 ± 1. 9	11.0 ± 1.9	**11.0 ± 1.9**
Katol-1	6.30	27.7 ± 2.7	30.7 ± 3.1	(9.27 ± 0.93)	29.2 ± 5	**30.4 ± 6.1**
Katol-2	4.91	29.3 ± 2.9	34.8 ± 3.5	(14.57 ± 1.46)	32.0 ± 5.4	
Katol-3	4.98	28.2 ± 2.8	32.1 ± 3.2	(13.51 ± 1.35)	30.1 ± 5.1	

T_3 stands for ^{3}He CRE ages, T_{21} for ^{21}Ne CRE ages, and T_{38} for ^{38}Ar CRE ages. All CRE ages are in million years (Ma). The indicated average CRE ages have been calculated using all or only part of the individual CRE ages. For clarity, we added parentheses to the ^{3}He and ^{38}Ar CRE ages that were not used in average calculation. The adopted CRE ages are indicated in bold characters in the last column. The given uncertainties are the standard deviations of the means (1σ).

shown in Appendix S2 in the supporting information (following, e.g., Barrat et al., 2012). For each of the analyzed meteorites, most of the element concentrations are in good agreement and consistent with an average H- and L-chondrite composition. Overall, the data show a reasonably good agreement between the major and minor elements' composition in three of the selected L6 meteorites, and the average L-chondrite composition; in order to overcome possible issues related to the (unknown) shielding depth of the meteorite samples, we consider the average L-chondrite composition for the further discussions. Indeed, the problem often lies in the fact that it is necessary to know the exact preatmospheric radius and the shielding depth of the sample in order to calculate the $^{21}Ne_{cos}$ production rate (P_{21}), which in most cases are unknown. In order to overcome this problem, the P_{21} has been estimated by a semi-empirical equation, based on the already existing correlations, and hence on average L/LL/H-chondrite chemical compositions. However, we use the determined U and Th concentrations to calculate the gas retention ages (see the Gas Retention Age section).

Cosmic Ray Exposure Ages

To calculate the CRE ages, we follow the same method as described in Li et al. (2017), based on Eugster (1988) and Dalcher et al. (2013), and use the concentrations of cosmogenic noble gases $^3He_{cos}$, $^{21}Ne_{cos}$, and $^{38}Ar_{cos}$; the calculated exposure ages are labeled as T_3, T_{21}, and T_{38}, respectively. To calculate CRE ages, we need to first calculate the production rates. However, such calculation requires knowing the exact preatmospheric radius and the shielding depth of the sample, which, in most cases, are unknown. Therefore, production rates were calculated using the average bulk chemical composition of L/H/LL chondrites and the cosmogenic Ne ratio $(^{22}Ne/^{21}Ne)_{cos}$ of each sample.

The production rate of $^3He_{cos}$ (P_3) is calculated using the formula given by Eugster (1988) (see Appendix S3 in the supporting information).

Likewise, to calculate the production rates of $^{21}Ne_{cos}$ (P_{21}), we used the model described in Dalcher et al. (2013), which links the production rates for cosmogenic $^{21}Ne_{cos}$ to the cosmogenic $(^{22}Ne/^{21}Ne)_{cos}$ ratios for chondrites (Appendix S3). Similarly, we determined the production rate of $^{38}Ar_{cos}$ (P_{38}) using the equation from Dalcher et al. (2013) (Appendix S3).

The CRE ages are all reported in Table 4; here, we will describe the CRE age results for each meteorite separately.

For the two Mangui duplicates, the calculated CRE ages vary between ~0.5 and 0.9 Ma; we observe the common trend $T_3 << T_{21} < T_{38}$; the T_3 is much lower, and consistent with significant ^3H and/or $^3He_{cos}$ diffusive losses, thus suggesting Mangui suffered severe heating after the breakup from its parent body and during its travel to Earth. Based on the "Bern plot" (Fig. 2), we estimate the diffusive losses to be in the range of ~54–75%. Based on this, we will not consider T_3 of Mangui any longer. The average of T_{21} and T_{38} for the two Mangui samples is 0.83 ± 0.13 Ma and 0.57 ± 0.09 Ma, the grand average and adopted age, calculated by simply averaging the two individual CRE ages for the two duplicates, being 0.70 ± 0.16 Ma. Figure 3a represents the compilation of CRE ages for L chondrites (Herzog & Caffee, 2014). We plot in red the four L6 chondrites measured by us. The CRE age of Mangui is shorter than any reported CRE age on the L-chondrite histogram. The CRE ages of Ozerki range between 1.00 and 1.42 Ma. Note that for Ozerki-2, T_{38} gives a CRE age of 0.55 ± 0.06 Ma, which is inconsistent with other ages and therefore ignored for

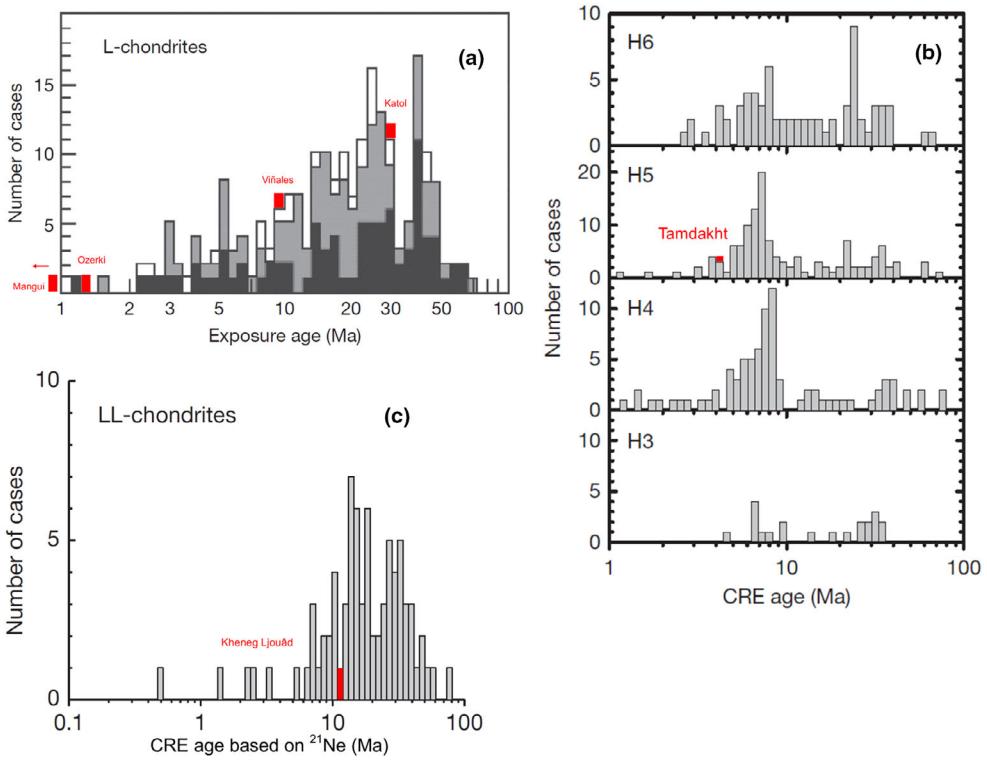

Fig. 3. Exposure ages of L (a), H (b), and LL (c) chondrites. The CRE ages of the samples measured by us appear in red. Reproduced and modified from Herzog and Caffee (2014) "Cosmic ray exposure ages of meteorites," Treatise on Geochemistry 2nd edition, Elsevier, pp. 419–454. With permission from Elsevier. (Color figure can be viewed at wileyonlinelibrary.com.)

the rest of the discussion. The CRE ages of two duplicates are consistent, with a grand average of 1.23 ± 0.34 Ma. The CRE age of Ozerki is in good agreement with the value of ~1.3–1.5 Ma calculated by Korochantseva et al. (2019). The calculated CRE ages of Viñales range between 8.1 and 10.4 Ma; as with Ozerki, the CRE ages of Viñales based on ^{38}Ar are systematically low compared to T_3 and T_{21}, by a factor of ~2. Thus, by omitting T_{38}, the grand average CRE age of Viñales is 9.4 ± 2.2 Ma.

The three duplicates of the Katol meteorite have CRE ages ranging from 28 ± 1 Ma to 33 ± 2 Ma, based on ^{3}He and ^{21}Ne only, the adopted CRE age being 30.4 ± 6.1 Ma. We observe the common trend $T_3 < T_{21}$ in all duplicates, which shows that a small amount of He has been lost during its CRE history. However, as in the case of Ozerki and Viñales, we notice that the calculated average CRE age based on the only cosmogenic $^{38}Ar_{cos}$ is too low by a factor of ~2.5 (i.e., 12 ± 2 Ma). The CRE ages of the Katol meteorite are consistent with one of the major peaks observed in the CRE age histogram of the L chondrites, around ~30 Ma (Fig. 3a) (e.g., Herzog, 2007; Herzog & Caffee, 2014; Marti & Graf, 1992).

The Tamdakht H5 meteorite has a CRE age that ranges between 2.59 and 3.37 Ma, with an adopted average CRE age of 3.02 ± 0.71 Ma. This age, although lower than the major peak centered around ~7 Ma (see Fig. 3b), confirms the common trend observed for H5 chondrites, with CRE ages slightly lower than for other petrologic types (Alexeev, 2001). The average CRE age of Tamdakht is slightly lower than the previously measured exposure age of 5.6 ± 0.4 (Alexeev et al., 2012). Such difference can be explained by evoking a large preatmospheric size, which would, therefore, make the ^{22}Ne/^{21}Ne ratio not applicable.

The CRE age of the LL5/6 Kheneg Ljouâd meteorite varies between 10.9 and 11.2 Ma, with a weighted average CRE age of 11.0 ± 1.9 Ma, based on all nuclides. This age is slightly lower but consistent with one of the peaks in the CRE age of the LL chondrites, with a major peak at ~15 Ma (see Fig. 3c) (e.g., Herzog & Caffee, 2014; Wieler, 2002).

Disagreements between CRE ages, and in particular with T_{38}, are frequently observed. Most recently, in the work of Di Gregorio et al. (2019), several samples from the well-studied LL/L5 chondrite Knyahinya have been measured for their noble gases. Although the powdered samples are thought to be representative of the bulk sample, cosmogenic $^{38}Ar_{cos}$ shows huge variations within the samples (i.e., ~66%), with a positive correlation between

$^{38}Ar_{cos}$ and Ca concentrations, Ca being one of the main target elements in the production of $^{38}Ar_{cos}$. Given that Ca concentrations are measured in different aliquots from the aliquots used for the noble gas measurements, Ca concentrations cannot be used to determine P_{38}.

Chemical heterogeneities in the distribution of the main target elements for the production of $^{38}Ar_{cos}$ are likely responsible for the observed variations in the $^{38}Ar_{cos}$ CRE ages of Viñales, Ozerki, and Katol.

A Possible L6 Crater Pairing?

One of the objectives of this work was to confirm whether or not the recent L6 falls Mangui, Ozerki, and Viñales could be crater paired. The two meteorites Mangui and Ozerki have CRE ages which, within their specific uncertainties, are not consistent with each other. It thus appears that Mangui and Ozerki are not paired. As for Viñales, with a weighted CRE age of 9.4 ± 2.2 Ma, it is not likely paired with Mangui and Ozerki. We can therefore conclude that the three shocked L6 chondrites Mangui, Viñales, and Ozerki have been produced by three different impacts on the L chondrite parent body(-ies) and are therefore not source crater paired.

Mangui: A Possible Link with Near-Earth Objects?

As mentioned earlier in the discussion, most of the ordinary chondrites have CRE ages in the range of 1–60 Ma (Herzog, 2007; Herzog & Caffee, 2014; Marti & Graf, 1992). However, in this study, two duplicates of Mangui (L6) chondrites have a nominal exposure age <1 Ma. Although rare for ordinary chondrites (OCs), CRE ages <1 Ma have already been calculated for several OCs, such as GRV 98004 (H5), Farmington (L5), Galim (LL6), or ALH82100 (CM2) (see Lorenzetti et al., 2003; Welten et al., 2015). Such low CRE ages, implying a really short parent body-Earth transfer, have been typically interpreted as an ejection occurring from a parent body already in an Earth-crossing orbit (e.g., Lorenzetti et al., 2003; Marti & Mathew, 2002; Welten et al., 2015, etc.). The evidence of a link between near-Earth objects (NEOs) or near-Earth asteroids (NEAs) and ordinary chondrites has been discussed in Binzel et al. (1996).

Mangui, having a nominal CRE age of ~0.6–0.8 Ma, based on both cosmogenic $^{3}He_{cos}$ and $^{21}Ne_{cos}$, is a possible candidate for an ejection event occurring from a parent body located in an Earth-crossing orbit (e.g., Apollo or Aten NEAs) rather than in the Main Belt. The massive loss of cosmogenic $^{3}He_{cos}$ observed in the two Mangui duplicates, probably by heating due to solar radiation, is an argument in favor of such a hypothesis.

Gas Retention Age

Gas retention ages are determined using the radiogenic $^{4}He_{rad}$ and $^{40}Ar_{rad}$ concentrations, and the abundances in the ^{238}U, ^{235}U, and ^{232}Th; parent isotopes of $^{4}He_{rad}$; and ^{40}K in the case of $^{40}Ar_{rad}$ (see Appendix S4 in the supporting information).

The concentrations in U, Th, and K used for the retention age calculations are taken as the average concentrations in L chondrites, that is, 13 ppb, 43 ppb, and 920 ppm, respectively, for Kheneg Ljouâd, Tamdakht, and Katol (Lodders & Fegley, 1998). For Mangui, Viñales, and Ozerki, we used the determined U and Th concentrations (see Appendix S1). For all calculations, we consider that the total amount of measured ^{40}Ar is radiogenic, all meteorites studied in this work being falls and therefore less affected by any atmospheric contribution; note, however, that such corrections for atmospheric ^{40}Ar might be more significant for meteorites with lower radiogenic amount, like Mangui and Viñales. The amount of radiogenic $^{4}He_{rad}$ is calculated by subtracting the amount of cosmogenic $^{4}He_{cos}$ from the total measured $^{4}He_{m}$. Assuming equal fractional losses of $^{3}He_{cos}$ and $^{4}He_{cos}$, the cosmogenic $^{4}He_{cos}$ is calculated as follows (Leya & Masarik, 2009):

$$^{4}He_{cos} = {}^{3}He_{cos} \times [(25.7 \pm 0.2) - (18.6 \pm 0.2) \times ({}^{22}Ne/{}^{21}Ne)_{cos}].$$

The nominal gas retention ages for all meteorites are presented in Table 5. The calculated ^{4}He (T_4) and ^{40}Ar (T_{40}) retention ages for Mangui range between ~3–9 Ma and ~88–108 Ma, respectively. The difference between T_4 and T_{40} in both of the Mangui samples can be explained by a preferential diffusion loss of $^{4}He_{rad}$ compared to $^{40}Ar_{rad}$. Such severe loss of radiogenic gases in Mangui could be explained by a collision event on the parent asteroid with an orbit closer to the Sun (rather than the only solar heating), therefore responsible of the fast delivery of Mangui to Earth (cf. see the Mangui: A Possible Link with Near-Earth Objects? section).

Regarding Ozerki, the similar trend $T_4 << T_{40}$ can be observed, suggesting again a preferential loss of radiogenic He. The Viñales U-Th-He and K-Ar retention ages are consistent with a severe shock about ~500 Ma ago, which is consistent with the catastrophic fragmentation of the L chondrite parent body, as shown in most of the L chondrites (e.g., Keil et al., 1994).

Figure 4 represents the ratio of the cosmogenic $^{3}He_{cos}$ and $^{21}Ne_{cos}$ exposure ages (T_3/T_{21}) versus the ratio of the gas retention ages (T_4/T_{40}).

The two Mangui duplicates plot above the 1:1 correlation line, indicating for both of them that a loss of

Table 5. Gas retention ages for the measured chondrites; T_4 stands for ^{4}He retention ages, T_{40} for ^{40}Ar retention ages.

Samples	$^4He_{rad}$ (10^{-8} cm^3 STP g^{-1})	T_4 (Ma)	$^{40}Ar_{rad}$ (10^{-8} cm^3 STP g^{-1})	T_{40} (Ma)
Mangui-1	3.411 ± 0.255	9 ± 1	43 ± 2	108 ± 11
Mangui-2	1.193 ± 0.089	3.12 ± 0.35	38 ± 2	88 ± 9
		(Ga)		(Ga)
Ozerki-1	593 ± 44	1.74 ± 0.18	6166 ± 308	4.25 ± 0.43
Ozerki-2	969 ± 72	2.61 ± 0.26	6499 ± 325	4.34 ± 0.44
		(Ma)		(Ma)
Viñales-1	178 ± 13	571 ± 59	221 ± 11	533 ± 55
Viñales-2	151 ± 11	486 ± 49	310 ± 16	707 ± 72
		(Ga)		(Ga)
Kheneg Ljouâd	1504 ± 112	3.53 ± 0.36	7437 ± 372	4.56 ± 0.46
Tamdakht	1466 ± 109	3.47 ± 0.36	5200 ± 260	3.97 ± 0.41
Katol-1	768 ± 57	1.51 ± 0.16	7716 ± 386	4.62 ± 0.47
Katol-2	428 ± 32	0.49 ± 0.05	5910 ± 296	4.18 ± 0.42
Katol-3	487 ± 36	0.71 ± 0.08	3916 ± 196	3.53 ± 0.37

The given T_4 and T_{40} uncertainties are the standard deviations of the means (1σ).

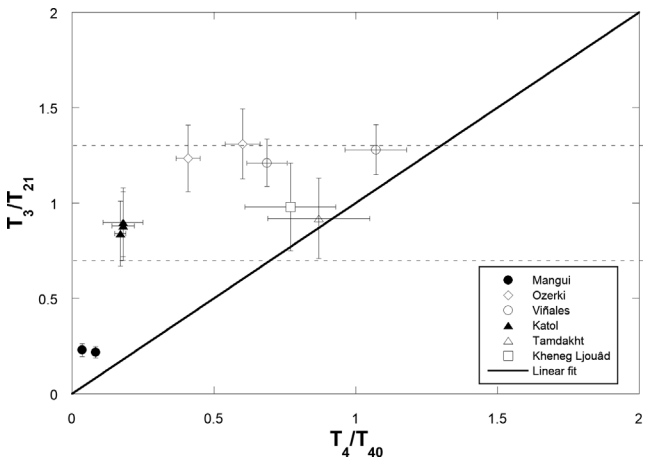

Fig. 4. Ratio of exposure ages (T_3/T_{21}) versus ratio of gas retention ages (T_4/T_{40}). Meteorites plotting on the solid line with slope 1 indicate no loss of ^{3}He and ^{4}He during their CRE age. Meteorites lying to the left of the solid line (i.e., Mangui) lost radiogenic $^4He_{rad}$ before their CRE age, either at or before breakup of their parent body. Data plotting in between the horizontal uncertainty dashed lines (i.e., Ozerki and Viñales) show no or only minor indications of ^{3}He and/or ^{3}H diffusive losses.

radiogenic $^4He_{rad}$ occurred before their exposure history, as well as ^{3}He diffusive losses. As for Ozerki and Viñales, both of them plot above the correlation line, with $T_3 > T_{21}$, but are within the uncertainty lines (dashed lines, Fig. 4), therefore indicating no or only minor diffusion losses.

The gas retention ages for Kheneg Ljouâd range between 3.53 and 4.56 Ga (T_4 and T_{40}, respectively), which shows that little radiogenic $^4He_{rad}$ has been lost during the CRE history of the meteoroid. A similar observation applies to the Tamdakht meteorite, its retention age varies between 3.47 ± 0.36 Ga and 3.97 ± 0.41 Ga. These ages are higher but consistent with previous data by Alexeev et al. (2012), with $T_4 = T_{40} = 3.1 \pm 0.3$ Ga. The good agreement between the two ages T_4 and T_{40} suggests no or only negligible loss of radiogenic gases during the exposure history. In addition, these two meteorites plot close to the 1:1 correlation line in Fig. 4, which further demonstrates that no or only minor diffusive losses of radiogenic gases occurred during their exposure histories.

As for the Katol L6 chondrite samples, their U-Th-He retention age varies between ~0.5 and ~1.5 Ga, whereas the ^{40}Ar retention age is in the range from ~3.5 to ~4.6 Ga, which is in good agreement with one of the main U-Th-He peak ages at ~0.5–1.0 Ga and with one of the K-Ar peak ages at ~4.2 Ga for L chondrites. The observed difference between the radiogenic $^4He_{rad}$ and $^{40}Ar_{rad}$ retention ages lies in the fact that helium has been preferentially lost during the CRE history of the meteorite.

SUMMARY AND CONCLUSIONS

We presented in this study a comprehensive noble gas investigation on recent ordinary chondrite falls. One of our goals was to determine whether or not the three recent L6 falls (Mangui, Viñales, and Ozerki) could be considered as crater paired. All results are summarized in Table 6.

Table 6. Best estimates of the CRE ages and gas retention ages for each of the studied meteorites.

Meteorite name	Type	Adopted CRE ages (Ma)	Retention ages (Ga)
Mangui	L6	0.70 ± 0.16	0.0031–0.108
Ozerki	L6	1.23 ± 0.34	1.74–4.34
Viñales	L6	9.39 ± 2.16	533–707
Katol	L6	30.4 ± 6.1	0.49–4.62
Kheneg Ljouâd	LL5/6	11.1 ± 1.9	3.53–4.56
Tamdakht	H5	3.24 ± 0.55	3.47–3.97

Adopted CRE ages: $T_{3,21,38}$ (see Table 4).
Retention ages: $T_{4,40}$.
The given age uncertainties are the standard deviations of the means (1σ).

1. First, based on their distinct CRE ages, Viñales is not source crater paired with both Mangui and Ozerki. In addition, based on their retention ages, Mangui and Ozerki are not paired. We can therefore conclude that the three shocked L6 chondrites Mangui, Viñales, and Ozerki have been produced by three different impacts on the L-chondrite parent body(-ies) and are therefore certainly not source crater paired.
2. Most of the CRE ages calculated by using the cosmogenic $^{38}Ar_{cos}$ concentrations are not consistent with the other dating schemes based on both cosmogenic $^{3}He_{cos}$ and $^{21}Ne_{cos}$ (e.g., in Ozerki, Viñales, Tamdakht, Kheneg Ljouâd, and Katol), therefore in agreement with the previous observations when doing measurements on small samples (~5–10 mg).
3. Kheneg Ljouâd (LL5/6) has a nominal CRE age of 11.0 ± 1.9 Ma, based on both cosmogenic $^{3}He_{cos}$ and $^{21}Ne_{cos}$. This age is shorter compared to one of the peaks in the CRE age histogram of the LL chondrites at ~15 Ma (e.g., Wieler, 2002).
4. The nominal CRE and gas retention ages of Tamdakht (H5) are consistent with previous observations for H5 chondrites. Its short CRE age (3.24 ± 0.55 Ma) compared to the major collision at 6–10 Ma reinforces the hypothesis of an age distribution for H chondrites dominated by small events occurring in several parent bodies (e.g., Herzog & Caffee, 2014).
5. The CRE age of the Mangui meteorite is shorter than 1 Ma, based on both $^{21}Ne_{cos}$ and $^{38}Ar_{cos}$. Such short CRE ages, although being rather unusual, have already been documented in a few ordinary chondrites (e.g., Lorenzetti et al., 2003; Marti & Mathew, 2002; Welten et al., 2015). To interpret such short exposure ages, one could evoke a delivery from a parent body in an Earth-crossing orbit (e.g., Binzel et al., 1996, 2002), as supported by the loss of cosmogenic $^{3}He_{cos}$ by heating due to solar radiation. Similarly, the observed severe loss of radiogenic gases in Mangui could be explained by a collision event on the parent asteroid with an orbit closer to the Sun (rather than an orbit in the Main Belt).

Acknowledgments—This work was supported by the SKL-K201802 funding grant from the State Key Laboratory of Lithospheric Evolution, IGGCAS, Beijing. The work of T. Smith was supported by the Chinese Academy of Sciences "President's International Fellowship Initiative" (PIFI). This work was also supported by the strategic priority program of the Chinese Academy of Sciences (#XDB41010205), the Civil Aerospace pre-research project (D020302), and the Key Deployment Projects of the Chinese Academy of Sciences (#ZDRW-KT-2019-5-5). We are grateful to the meteorite hunter Mr. Shu Yin for generously providing Ozerki and Viñales samples. We also thank G. Herzog, K. Metzler, three anonymous reviewers, and the associate editor M. Caffee who both provided detailed and constructive reviews that considerably helped in improving the paper.

Conflicts of interest—The authors declare no conflicts of interest.

Data Availability Statement—Data openly available in a public repository that issues data sets with DOIs.

Editorial Handling—Dr. Marc Caffee

REFERENCES

Alexeev, V. A. 1998. Parent Bodies of L and H Chondrites: Times of Catastrophic Events. *Meteoritics & Planetary Science* 33: 145–52.

Alexeev, V. A. 2001. Some Peculiarities of H-Chondrite Parent Body Evolution. *Solar System Research* 35: 458–68.

Alexeev, V. A., V. D. Groin, A. I. Ivliev, L. L. Kashkarov, U. Ott, D. A. Sadilenko, and G. K. Ustinova. 2012. Integrated Study of the Thermoluminescence, Noble Gases, Tracks, and Radionuclides in the Fresh-Fallen Ash Creek L6 and Tamdakht H5 Chondrites. *Geochemistry International* 50(2): 105–24.

Aoudjehane Chennaoui, H., and L. A. J. Garvie. 2018. Kheneg Ljouâd (Morocco): The Unique LL5/6 Meteorite Fall (Abstract #2067). 81st Annual Meeting of the Meteoritical Society.

Barrat, J. A., B. Zanda, F. Moynier, C. Bollinger, C. Liorzou, and G. Bayon. 2012. Geochemistry of CI Chondrites: Major and Trace Elements, and Cu and Zn Isotopes. *Geochimica et Cosmochimica Acta* 83: 79–92.

Bhandari, N., D. Lal, R. S. Rajan, J. R. Arnold, K. Marti, and C. B. Moore. 1980. Atmospheric Ablation in Meteorites: A Study Based on Cosmic Ray Tracks and Neon Isotopes. *Nuclear Tracks* 4: 213–62.

Binzel, R. P., D. F. Lupishko, M. Di Martino, R. J. Whiteley, and G. J. Hahn. 2002. Physical Properties of Near-Earth Objects. In *Asteroids III*, edited by W. F. Bottke, A. Cellino, P. Paolicchi, and R. P. Binzel, 255–71. Tucson, Arizona: The University of Arizona Press.

Binzel, R. P., J. B. Schelte, T. H. Burbine, and J. M. Sunshine. 1996. Spectral Properties of Near-Earth Asteroids: Evidence for Source of Ordinary Chondrite Meteorites. *Science* 273: 946–8.

Dalcher, N., M. W. Caffee, K. Nishiizumi, K. C. Welten, N. Vogel, R. Wieler, and I. Leya. 2013. Calibration of Cosmogenic Noble Gas Production in Ordinary Chondrites Based on ^{36}Cl-^{36}Ar Ages. Part 1: Refined Produced Rate for Cosmogenic ^{21}Ne and ^{38}Ar. *Meteoritics & Planetary Science* 48: 1841–62.

Di Gregorio, M., H. Busemann, A. C. Hunt, D. Krietsch, M. Schönbächler, and C. Maden. 2019. Variable Cosmogenic Argon in L/LL5 Chondrite Knyahinya. 82nd Annual Meeting of the Meteoritical Society.

Efimov, A. V., A. P. Kartashova, and A. K. Murtazov. 2019. Visual Spectrum of Chondrite L6 Meteorite Ozerki. 82nd Annual Meeting of the Meteoritical Society.

Eggins, S. M., J. D. Woodhead, L. P. J. Kinsley, G. E. Mortimer, P. Sylvester, M. T. McCulloch, J. M. Hergt, and M. R. Handler. 1997. A Simple Method for the Precise Determination of ≥40 Trace Elements in Geological Samples by ICPMS Using Enriched Isotope Internal Standardization. *Chemical Geology* 134: 311–26.

Eugster, O. 1988. Cosmic-Ray Production Rates for ^{3}He, ^{21}Ne, ^{38}Ar, ^{83}Kr, and ^{126}Xe in Chondrites Based on ^{81}Kr-Kr Ages. *Geochimica et Cosmochimica Acta* 52: 1649–62.

Gattacceca, J., F. M. McCubbin, A. Bouvier, and J. Grossman. 2020a. The Meteoritical Bulletin, No. 107. *Meteoritics & Planetary Science* 55: 460–2.

Gattacceca, J., F. M. McCubbin, A. Bouvier, and J. Grossman. 2020b. The Meteoritical Bulletin, No. 108. *Meteoritics & Planetary Science* 55: 1146–50.

Herzog, G. F. 2007. Cosmic-Ray-Exposure Ages of Meteorites. In Treatise on Geochemistry, edited by H. D. Holland and K. K. Turekian, 1–36. Amsterdam: Elsevier.

Herzog, G. F., and M. W. Caffee. 2014. Cosmic-Ray-Exposure Ages of Meteorites. In Treatise on Geochemistry, 2nd ed., edited by A. M. Davis, 419–54. Amsterdam: Elsevier.

Ji, J. L., S. Hu, Y. T. Lin, Q. Zhou, and Y. Xiao. 2018. Petrography, Mineral Chemistry and Shock Metamorphism of the Mangui Meteorite. *Chinese Science Bulletin* 64: 579–87. In Chinese with English abstract.

Jull, A. J. T. 2001. Terrestrial Ages of Meteorites. In *Accretion of Extraterrestrial Matter Throughout Earth's History*, edited by B. Peucker-Ehrenbrink and B. Schmitz, 241–66. Boston, MA: Springer.

Kamber, B. S., A. Greig, R. Schoenberg, and K. D. Collerson. 2003. A Refined Solution to Earth's Hidden Niobium: Implications for Evolution of Continental Crust and Depth of Core Formation. *Precambrian Research* 126: 289–308.

Keil, K., H. Haack, and E. R. D. Scott. 1994. Catastrophic Fragmentation of Asteroids: Evidence from Meteorites. *Planetary and Space Science* 42: 1109–22.

Korochantseva, E. V., A. B. Verchovsky, C. A. Lorenz, A. I. Buikin, and A. V. Korochantsev. 2019. The Ozerki Meteorite: Petrology and the First Data on Noble Gases and Nitrogen Released by Stepwise Combustion and Crushing Methods. 82nd Annual Meeting of the Meteoritical Society.

Lavielle, B., K. Marti, J.-P. Jeannot, K. Nishiizumi, and M. Caffee. 1999. The ^{36}Cl-^{36}Ar-^{40}K-^{41}K Records and Cosmic Ray Production Rates in Iron Meteorites. *Earth and Planetary Science Letters* 170: 93–104.

Leya, I., K. Ammon, M. Cosarinsky, N. Dalcher, E. Gnos, B. Hofmann, and L. Huber. 2013. Light Noble Gases in 12 Meteorites from the Omani Desert, Australia, Mauritania, Canada, and Sweden. *Meteoritics & Planetary Science* 48: 1401–14.

Leya, I., and J. Masarik. 2009. Cosmogenic Nuclides in Stony Meteorites Revisited. *Meteoritics & Planetary Science* 44: 1061–86.

Li, B. P., A. Greig, J. X. Zhao, K. D. Collerson, K. S. Quan, Y. H. Meng, and Z. L. Ma. 2005. A New Estimate for the Composition of Weathered Young Upper Continental Crust from Alluvial Sediments, Queensland, Australia. *Geochimica et Cosmochimica Acta* 69: 1041–58.

Li, S., W. Luo, B. Li, and Y. Li. 2020. The Survey of Mangui Meteorite Shower in Xishuangbanna, Yunnan Province. *Acta Mineralogica Sinica* 40: 176–82. In Chinese with English abstract.

Li, S., S. Wang, I. Leya, Y. Li, X. Li, and T. Smith. 2017. Petrology, Mineralogy, Porosity, and Cosmic-Ray Exposure History of Huaxi Ordinary Chondrite. *Meteoritics & Planetary Science* 52: 937–48.

Lodders, K., and B. Fegley Jr. 1998. *The Planetary Scientist's Companion*. New York: Oxford University Press.

Lorenzetti, S., Y. Lin, D. Wang, and O. Eugster. 2003. Noble Gases and Mineralogy of Meteorites from China and the Grove Mountains, Antarctica: A 0.05 Ma Cosmic Ray Exposure Age of GRV 98004. *Meteoritics & Planetary Science* 38: 1243–53.

Marti, K., and T. Graf. 1992. Cosmic-Ray Exposure History of Ordinary Chondrites. *Annual Review of Earth and Planetary Sciences* 20: 221–43.

Marti, K., and K. J. Mathew. 2002. Near-Earth Asteroid Origin for the Farmington Meteorite (abstract #1132). 33rd Lunar and Planetary Science Conference. CD-ROM.

Matsuda, J., T. Matsumoto, H. Sumino, K. Nagao, J. Yamamoto, Y. Miura, I. Kaneoka, N. Takahata, and Y. Sano. 2002. The ^{3}He/^{4}He Ratio of the New Internal He Standard of Japan (HESJ). *Geochemical Journal* 36: 191–5.

Moniot, R. K., T. H. Kruse, C. Tuniz, W. Savin, G. S. Hall, T. Milazzo, D. Pal, and G. F. Herzog. 1983. The ^{21}Ne Production Rate in Stony Meteorites Estimated from ^{10}Be and Other Radionuclides. *Geochimica et Cosmochimica Acta* 47: 1887–95.

Nishiizumi, K., S. Regnier, and K. Marti. 1980. Cosmic Ray Exposure Ages of Chondrites, Pre-Irradiation and Constancy of Cosmic Ray Flux in the Past. *Earth and Planetary Science Letters* 50: 156–70.

Ranjith, P. M., H. He, B. Miao, F. Su, C. Zhang, Z. Xia, L. Xie, and R. Zhu. 2017. Petrographic Shock Indicators and Noble Gas Signatures in a H and an L Chondrite from Antarctica. *Planetary and Space Science* 146: 20–9.

Ray, D., S. Ghosh, and S. V. S. Murty. 2017. On the Possible Origin of Troilite-Metal Nodules in the Katol Chondrite (L6–7). *Meteoritics & Planetary Science* 52: 72–88.

Ruzicka, A., J. Grossman, A. Bouvier, C. D. K. Herd, and C. B. Agee. 2015. The Meteoritical Bulletin, No. 102. *Meteoritics & Planetary Science* 50: 1662.

Shaviv, N. J. 2002. Cosmic Ray Diffusion from the Galactic Spiral Arms, Iron Meteorites, and a Possible Climatic

Connection. *Physical Review Letters* 89, 089901. https://doi.org/10.1103/Phys.RevLett.89.051102.
Shaviv, N. J. 2003. The Spiral Structure of the Milky Way, Cosmic Rays, and Ice Age Epochs on Earth. *New Astronomy* 8: 39–77.
Smith, T., D. L. Cook, S. Merchel, S. Pavetich, G. Rugel, A. Scharf, and I. Leya. 2019. The Constancy of Galactic Cosmic Rays as Recorded by Cosmogenic Nuclides in Iron Meteorites. *Meteoritics & Planetary Science* 54: 2951–76.
Vogt, S. K., D. Aylmer, G. F. Herzog, R. Wieler, P. Signer, P. Pellas, C. Fiéni et al. 1993. On the Bur Gheluai H5 Chondrite and Other Meteorites with Complex Exposure Histories. *Meteoritics* 28: 71–85.
Weisberg, M. K., C. Smith, G. Benedix, L. Folco, K. Righter, J. Zipfel, A. Yamaguchi, and H. Aoudjehane Chennaoui. 2009. The Meteoritical Bulletin, No. 95. *Meteoritics & Planetary Science* 44: 429–62.
Welten, K. C., M. W. Caffee, M. M. M. Meier, M. Riebe, K. Nishiizumi, and R. Wieler. 2015. The Short Cosmic Ray Exposure Ages of Two H Chondrites: Evidence of a Common Ejection Even 0.1 Million Years Ago (abstract #2866). 46th Lunar and Planetary Science Conference. CD-ROM.
Wieler, R. 2002. Noble Gases in the Solar System. In *Noble Gases in Geochemistry and Cosmochemistry*, edited by D. Porcelli, C. Ballentine, and R. Wieler, 21–70. Reviews in Mineralogy and Geochemistry, vol. 47. Washington, D.C.: Mineralogical Society of America.
Wieler, R., J. Beer, and I. Leya. 2013. The Galactic Cosmic Ray Intensity Over the Past 10^6–10^9 Years as Recorded by Cosmogenic Nuclides in Meteorites and Terrestrial Samples. *Space Science Reviews* 176: 351–63.
Yin, F., and D. Dai. 2021. Petrology and Mineralogy of the Viñales Meteorite, the Latest Fall in Cuba. *Science Progress* 104: 1–12.

SUPPORTING INFORMATION

Additional supporting information may be found in the online version of this article.

Appendix S1. Major and minor elements in the measured meteorites measured by ICP-MS.

Appendix S2. Distribution of the majorand minor elements in the Mangui, Viñales, and Ozerki meteorites.

Appendix S3. Calculation of cosmogenic noble gas production rates and exposure ages.

Appendix S4. U-Th-He and K-Ar retention ages calculation.